Composites Science and Technology 74 (2013) 6–13

Contents lists available at SciVerse ScienceDirect

Composites Science and Technology

journal homepage: www.elsevier.com/locate/compscitech

SiC formation on carbon nanotube surface for improving wettability with aluminum

Kang Pyo So [a], Jun Cheol Jeong [b], Jong Gil Park [b], Hyoen Ki Park [b], Yong Ho Choi [b], Dong Hwan Noh [b], Dong Hoon Keum [a], Hye Yun Jeong [a], Chandan Biswas [a], Chan Ho Hong [b], Young Hee Lee [a,*]

[a] BK21 Physics Division, Department of Energy Science, Center for Nanotubes and Nanostructured Composites, Sungkyunkwan University, Suwon 440-746, South Korea
[b] Material Research Team, Dayou Smart Aluminium Co., Ltd., Wanju-gun 565-902, South Korea

ARTICLE INFO

Article history:
Received 1 June 2012
Received in revised form 17 August 2012
Accepted 18 September 2012
Available online 3 October 2012

Keywords:
A. Carbon nanotubes
B. Interfacial strength
D. Transmission electron microscopy
E. Casting
Wettability

ABSTRACT

High interfacial strength between the host matrix and reinforcing material is the key factor in developing mechanically robust composite materials. Strengthening the interface between aluminum and carbon nanotubes (CNTs) is very crucial to achieve desirable mechanical properties of Al-CNT composites. Silicon carbide that highly wets Al was coated on the CNT surface in order to promote interfacial strength while preventing CNT disintegration during reinforcement. The SiC interface layer on the CNT surface was successfully formed by a three-step process: (i) mechanical crushing of a Si powder by a CNT promoter, (ii) coating of crushed Si nanoparticles onto CNT surfaces, and (iii) formation of a SiC layer by high temperature annealing. The wettability of CNTs during Al melting was significantly improved by this method, which is critical for improving mechanical properties of Al-CNT composites. Improvements of 15% in tensile strength and 79% in Young's modulus were achieved by adding 0.84 wt% Si powder and 1 wt% CNTs.

1. Introduction

Carbon nanotubes (CNTs) with extraordinary mechanical, thermal, and electrical properties have been used to improve the properties of polymer, metal, and ceramic composites [1–7]. The composite performance is strongly dependent on the dispersion, length, crystallinity, and degree of alignment of the CNTs, as well as the characteristics of the interface between the CNT surface and host materials.

Mechanically strong metal composites have attracted interest recently due to green energy requirements [8]. Although aluminum is a known rust-free light material and is used in car wheels and window frames, its use is still limited mainly due to its poor mechanical strength compared to that of iron. A CNT-based aluminum composite with enhanced mechanical strength could be utilized to improve the fuel efficiency of vehicles by reducing their weight. Its application may be further extended to electronic parts, ships, aircraft and satellites. Therefore, the robust formation of CNT-aluminum composites with high mechanical strength is desired.

However, difficulties arise because of distinct differences in the physical properties of aluminum and CNTs [9]. The large difference in surface tension and mass density are the cause of inhomogeneous dispersion of CNTs within a metal matrix [10–12]. For instance, aluminum has a surface tension of 955 mN/m at its melting temperature [13], much higher than the 45.3 mN/m of CNTs [14]. This suggests that aluminum cannot sufficiently wet the CNT surface. The poor wettability problem could be improved by formation of Al_4C_3 between CNTs and aluminum [15]. However, thermal degradation is a serious problem arising from the strong chemical reaction between CNTs and aluminum above the Al melting temperature [16,17]. This destroys the structure of CNTs, forming an unstable Al_4C_3 phase, which deteriorates the mechanical properties.

This issue could be solved by decorating the surfaces of CNTs with ceramics, for example, silicon carbide (SiC) [19]. The aluminum contact angle on a SiC substrate was found to be significantly lower (60° at equilibrium) than that on a carbon substrate (165° before aluminum and carbon reaction) [15,18]. This implies that a SiC coating on CNTs could decrease the contact angle and improve wettability to Al. At the same time, the SiC coating layer could prevent the oxidation from air and Al–C reaction from matrix [19,20]. Another advantage of using such a precursor is the potential for improved interfacial strength at the interface by the formation of a covalent SiC bond [15,21]. The mechanical properties could be improved by high external load transfer to the CNTs through the interfacial covalent bond. Furthermore, a stable SiC layer can prevent structural degradation of CNTs from the aluminum matrix. However, thermodynamic analysis of the formation of Al_4C_3 on CNTs in an Al–Si alloy matrix shows a favorable aluminum–carbon reaction [22]. This result suggests that Si incorporation into the matrix does not form a SiC layer on the CNT

* Corresponding author. Address: Department of Physics, Sungkyunkwan University, Suwon 440-746, South Korea. Tel.: +82 31 299 6507.
E-mail address: leeyoung@skku.edu (Y.H. Lee).

0266-3538/$ - see front matter
http://dx.doi.org/10.1016/j.compscitech.2012.09.014

surface. Therefore, the formation of a SiC layer on CNTs is more desirable prior to mixing with aluminum.

In this study we introduced a SiC layer on the CNT surface prior to incorporation into the aluminum matrix. The SiC layer was synthesized by a three-step process: (i) mechanical crushing of Si powder by a CNT promoter, (ii) coating the CNT surface with crushed Si nanoparticles, and (iii) formation of a SiC layer by high temperature annealing. The morphologies and microstructures of SiC formation were investigated by scanning electron microscopy (SEM) and transmission electron microscopy (TEM), which indicated successful decoration of a SiC layer on the CNTs. X-ray diffraction confirmed the formation of a SiC lattice. Thermal properties were analyzed by thermogravimetric analysis (TGA), which revealed an increase in oxidation temperature. Improvements in aluminum wettability were investigated by measuring the contact angle by a sessile drop method. The mechanical properties were also characterized by tensile and hardness testing after fabrication of a SiC/CNT-A356.2 composite by a melt blending technique.

2. Material and methods

2.1. Formation of a SiC layer on MWCNTs

The diameter and length of the multi-walled (MW) CNTs (CM95, Hanwha Nanotech, Korea) were in the range of 10–30 nm and a few tens of micrometers, respectively. A 1:1 atomic ratio mixture (7:3 by weight ratio) of Si powder (325 mesh, 99%, Aldrich) to MWCNTs were mechanically crushed by means of a planetary ball miller (Pulverisette 6, Fristch, Germany) for 10 h at 230 rpm with 5 mm zirconia balls. Additional MWCNTs were added to this crushed mixture. Different mixing ratios (3:5, 6:5, 12:5 and 20:5) of the crushed mixture to MWCNTs were investigated. In order to form SiC on the MWCNT surfaces (SiC/CNT), high temperature annealing was performed at 1300 °C for an hour in a vacuum induction furnace.

2.2. Wetting angle measurement

Raw MWCNTs and SiC/CNT powder were pelletized to 15 mm in diameter and 3 mm in thickness by pressurizing at 500 MPa using a press punch at room temperature. A smooth surface of the CNT pellet was achieved using a micro mechanically polished press punch. Pure aluminum melt (99%, 0.35 cc of volume) was poured on the specially designed iron mesh supporter where a naturally formed oxide layer from the outer surface of the Al droplet was filtered in a vacuum. A pure liquid Al droplet was precipitated on top of the CNT pellet at 800 °C for 5 min under vacuum at 10^{-2} torr pressure. The contact angle of the interface between the Al droplet and CNT pellet was characterized using a camera (IXUS 99015, canon).

2.3. Fabrication of SiC/CNT and A356.2 composite

In order to test the mechanical properties of the Al composite with SiC/CNTs, A356.2 casting alloy was used as a matrix. The SiC/CNTs-A356.2 composite was fabricated by a melt blending technique with a pretreatment process. The process was carried out in three steps: (i) ball milling to mix pure aluminum powder with SiC/CNTs, (ii) melt blending with A356.2, and (iii) die casting of tensile measurement specimens. For this, 5 wt% SiC/CNTs were mixed with Al powder (Samjeon Chemicals, Korea) by ball milling for 5 h. The melt blending was conducted by melting the SiC/CNT-aluminum granular mixture at 650 °C in vacuum ($\sim 10^{-3}$ torr) while stirring with a graphite impeller. The tensile strength measurement specimen of SiC (1.2 wt%)/CNT (1 wt%)-A356.2 composite was fabricated by die casting (TOYO 250, Toyo, Japan). An ASTM E 8M-08 standard die casting specimen was used for tensile strength measurement. To ensure accurate measurement, the inner side gate of the specimen after die casting was used for hardness testing after T6 heat treatment in an air environment. Solution temperatures and aging conditions were 470–560 °C for 4 h and 130 °C for 3 h, respectively.

2.4. Measurement

The morphology of SiC/CNTs was characterized by field-emission SEM (FESEM, 6700F, JEOL) and high resolution TEM (HRTEM, 2010F, JEOL, 200 keV). Elemental analysis was performed by energy dispersive X-ray spectroscopy (EDS). Formation of SiC bonding was characterized by means of X-ray diffraction (XRD, Rigaku Rotaflex D/MAX system, Rigaku, Japan, Cu Kα, 1.54 Å) and thermogravimmetric analyzer (TGA, Q500, TA instrument) measurements. Mechanical properties were measured using an ultimate tensile tester (UTM, DTU-900MH, Deakyung tech & tester MTG, Korea, 3t) and a micro Vickers hardness tester (Hardness, 810-351K, Mitutoyo, Japan).

3. Results and discussion

3.1. Formation of SiC on the CNT surface

A schematic illustrating the procedure for SiC formation on a CNT surface is shown in Fig. 1. In Step I, mechanical ball milling was done to crush Si particles with the CNT promoter. While CNTs disintegrated into a carbon source for SiC formation, CNTs also promoted crushing of the Si particles to nanoscale sizes. The atomic ratio of Si:CNTs was 1:1; equivalent for SiC formation (7:3 in terms of weight ratio). In order to ensure sufficient crushing, the ball milling time was maintained for 10 h. Fig. 1a shows the mechanically crushed Si particles and CNT flakes. The Si particles were mixed with fragmented CNT flakes. In Step II, additional MWCNTs were mixed with a crushed Si-CNT flake mixture by ball milling for an hour, as shown in Fig. 1b. In this process, the crushed Si particles were coated on additional CNT surfaces. In Step III, SiC bond formation on the CNT surface was achieved with high temperature annealing at 1300 °C for an hour in vacuum, as shown in Fig. 1c. Schematic and TEM images of a SiC layer on CNTs are shown in Fig. 1c. No significant structural damage in CNT was observed in the TEM characterization.

3.2. Morphology of SiC on CNTs

The morphology of SiC formed on the CNT surface was examined for each step by FESEM (Fig. 2). Raw MWCNTs with their entangled structure and Si particles with an average diameter of 10 μm were observed, as shown on the left and right sides of Fig. 2a, respectively. The crushed mixture of Si particles and MWCNTs (Step I) is shown in Fig. 2b. The CNT structure was clearly observed throughout the whole sample. The particle size distribution of the crushed Si/CNT mixture was observed to be larger than ten micrometers. The structure implies that Si and CNTs were totally blended via high energy mechanical crushing. Short MWCNTs were observed, approximately 100–200 nm in length, which indicated mechanical damage to the CNTs during high energy mechanical crushing. Rough surfaces of the CNT flakes were observed in this case, which could have resulted from the deposition of fine Si nanoparticles.

Fig. 2c shows the SEM micrograph of MWCNTs coated with the crushed mixture. The mixing ratio of the crushed mixture to

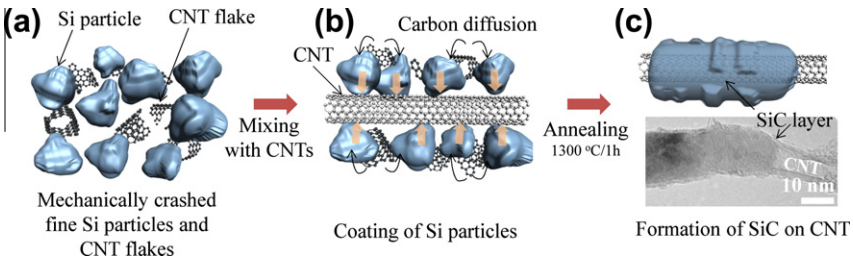

Fig. 1. Schematic showing the procedure for SiC formation on the CNT surface. (a) Mechanically crushed fine Si particles and CNT flakes, (b) coating of Si particles on CNT, and (c) TEM image showing the formation of a SiC layer on the CNTs.

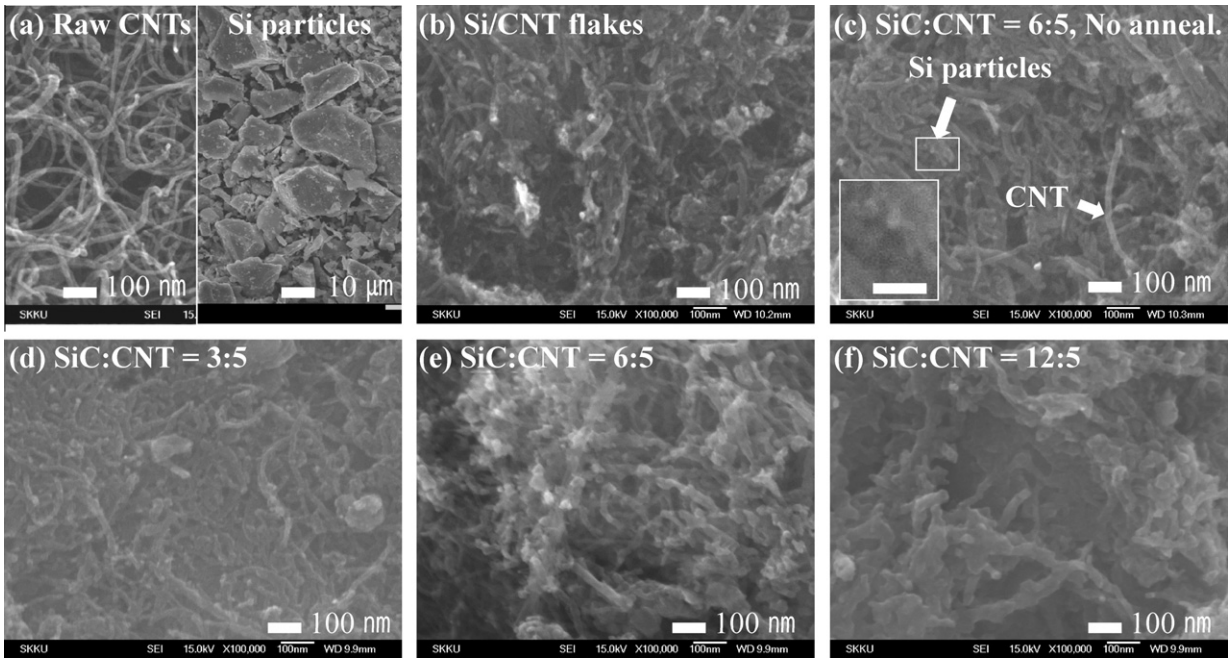

Fig. 2. SEM images for each step of SiC formation on CNTs. (a) Raw MWCNTs, (b) mechanically crushed fine Si particles and CNT flakes, (c) mixture of SiC:CNT = 6:5 before annealing. Inset: crushed fine Si particles (scale bar is 50 nm). Formation of a SiC layer on CNTs after annealing at a mixing ratio of SiC:CNT = (d) 3:5, (e) 6:5, and (f) 12:5.

MWCNTs (Step II) was 6:5. The presence of long CNTs and crushed fine Si particles (as shown in the inset) was clearly visible, indicating successful mixing in Step II. High temperature annealing could result in SiC formation (from the crushed Si/CNT mixture) on the MWCNT surface at 1300 °C for 1 h (Step III). Fig. 2d shows SiC/CNT at a mixing ratio of 3:5 after annealing. One interesting fact relating to the CNT surface properties can be observed in these SEM micrographs. Before annealing (Step III), CNTs were semi-transparent in SEM micrographs (Fig. 2a and c). However, after annealing, the CNT surface became rougher and the strands became totally opaque under an electron beam (as shown in Fig. 2d). These phenomena indicate that the surface properties were changed after annealing, suggesting the formation of SiC layers on the CNT surface, and were more obvious at a high SiC concentration (Fig. 2e and f at mixing ratios of 6:5 and 12:5, respectively). The diameter of CNTs at a mixing ratio of 12:5 increased to approximately 50 nm, which is more than twice that of the raw MWCNTs (Fig. 2f).

3.3. Microstructure and lattice diffraction analysis of the SiC layer

The structural properties of SiC-coated CNTs were investigated by TEM, as shown in Fig. 3. The TEM image indicated an increase in CNT diameters up to nearly 40 nm (Fig. 3a), implying successful SiC layer coating on the CNT surface. The area indicated by a white box in Fig. 3a was further characterized with high resolution TEM in order to understand the SiC-coated CNT microstructure in detail (Fig. 3b). The graphitic layered structure of the CNT walls was clearly visible in this magnified image (right middle inset), confirming that the CNT structure was preserved, as mentioned earlier. The thickness of the SiC layer on the CNT surface was observed to be around 10 nm. Selected area electron diffraction (SAED) was performed on the coated SiC layer to investigate its crystalline properties (right bottom inset). SAED clearly showed a dotted pattern, highlighting the crystalline nature of the SiC layer formed on the CNT surface. Element mapping was also performed by EDS for the area indicated by a white square in Fig. 3a in order to investigate the Si elemental distribution (Fig. 3c). The results clearly indicated the material deposited around the CNT surface was Si, consistent with previous observations shown in Fig. 2. The concentrations of C, Si, and O were observed in the spectrum, as shown in Fig. 3d. The Cu peak was excluded from the observation because it was only from the Cu TEM grid. The concentrations of C, Si and O were 49, 45, and 6 wt%, respectively.

Furthermore, the formation of crystalline SiC was verified by XRD (Fig. 4). Crystalline Si peaks were only observed before anneal-

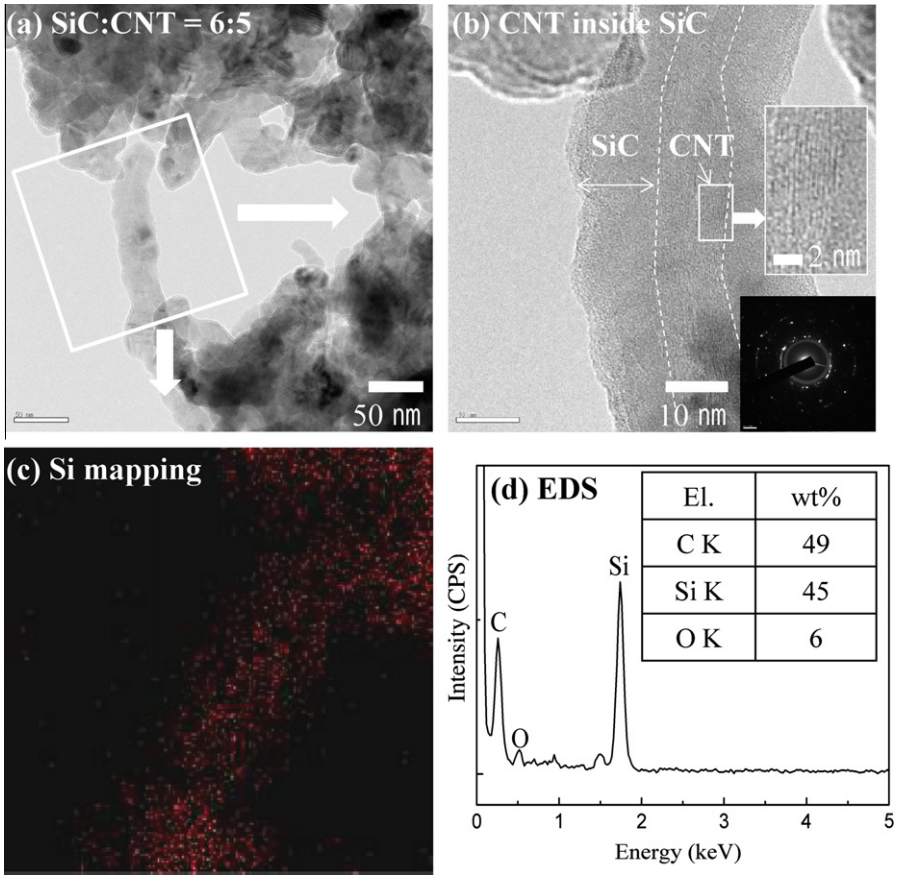

Fig. 3. Microstructural observation of the SiC layer on the CNT surface after annealing. TEM image of (a) the SiC layer formed on CNTs at a SiC:CNT ratio of 6:5, and (b) CNT structure inside the SiC coating. Inset: CNT wall structure (right middle) and SAED pattern (right bottom). (c) Si element mapping for the area indicated by a white square in (a), and (d) EDS analysis.

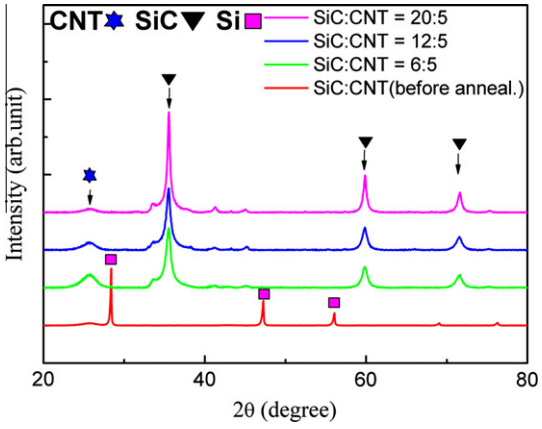

Fig. 4. XRD analysis of SiC formation after annealing.

ing of the SiC/CNT samples (bottom red[1] curve). However, after annealing at high temperature, the presence of crystalline SiC was confirmed by the sharp peaks at 35.6°, 60.2°, and 71.7°, which could originate from the [1 1 1], [2 2 0], and [3 1 1] planes of face-centered-cubic SiC (black triangle), respectively [23]. All of the Si crystal peaks disappeared from the annealed samples and similar SiC peaks were repeatedly observed in samples with different SiC:CNT input ratios. A previous investigation showed that Si reacts with CNTs above 1000 °C [24]. Our result findings suggest the total conversion of Si to SiC, in agreement with the previous results. Therefore, the formation of a SiC crystal on the CNT surface observed in the TEM images was verified by this XRD analysis.

3.4. Thermal analysis of SiC formation by TGA

Thermal properties and quantitative SiC formation were analyzed for each experimental step by TGA. Pristine MWCNTs started to burn and decrease in overall weight from 500 °C, as shown in Fig. 5a. In contrast, the CNT flakes present in the crushed Si and the CNT mixture started burning around 300 °C due to the high structural damage during mechanical crushing. The amount of burned CNT flakes was 29.3%, close to the 30% input MWCNTs. No SiC was formed during mechanical crushing. The amount of CNTs burned increased to 55.2 wt% after mixing with additional CNTs, smaller than the input amount of CNTs (61.8 wt%). This small difference might originate from partial disintegration of CNTs during the mixing process. Crushed CNT flakes can be converted to SiC crystals after high temperature annealing, and this conversion process could have resulted in the reduction in the amount of CNT burned up to 38 wt%, as indicated by the TGA measurements. The onset of the CNT burning temperature also increased up to 660 °C. The SiC formed on the CNT surface could protect the CNTs from oxygen, resulting in increased oxidation temperature [20]. The amount of crushed CNT flakes and additional non-crushed CNTs was calculated by dW/dT from the TGA curve before annealing, as shown in Fig. 5b. At 650 °C, nearly all of the CNT content

[1] For interpretation of color in Fig. 4, the reader is referred to the web version of this article.

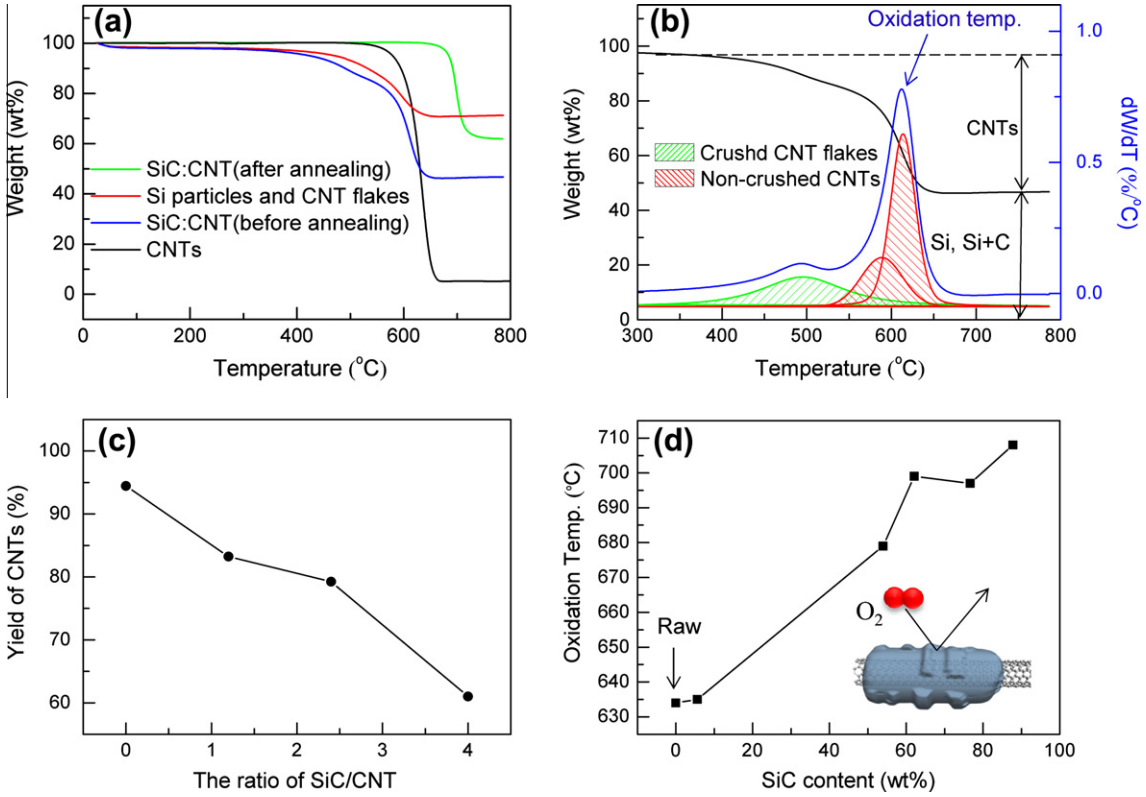

Fig. 5. Thermal analysis of SiC formation by TGA. (a) TGA in air for each process and (b) TGA and deconvolution of differential TGA for an SiC:CNT ratio of 6:5. (c) The yield of CNTs after annealing. (d) The change in oxidation temperature as a function of the amount of SiC.

burned, and the remaining 44.8 wt% could be related to the Si, a mixture of Si and disintegrated C originating during the ball milling process. The differential TGA curve was deconvoluted with a combination Lorentzian and Gaussian function, as shown in Fig. 5b. The peak was divided into crushed CNT flakes and non-crushed CNTs. Crushed CNT flakes with high structural damage showed a lower burning temperature around 495 °C [25]. Other peaks were observed at higher temperatures around 590 and 610 °C. These peaks were considered to originate from non-crushed CNTs in Step II. The quantity of crushed CNT flakes and non-crushed CNTs was calculated from the integration of these peaks. The integrated value of the crushed CNT flakes and non-crushed CNTs was 31.4% and 68.5%, respectively. The amount of non-crushed CNTs was relatively smaller than the input CNT value (73.5%). This difference could be the result of structural damage to the CNTs during mechanical mixing.

The yield of CNTs was also determined after high temperature annealing. Fig. 5c shows the yield of CNTs versus the input SiC/CNTs ratio. The yield of CNTs was calculated from the amount burned per input non-crushed CNTs. The yield of CNTs decreased as the ratio of SiC/CNTs increased. This indicates that some of the non-crushed CNTs participated in SiC formation. Fig. 5d shows the oxidation temperature of CNTs versus SiC content. The oxidation temperature was obtained from the peak maximum of the differential TGA curve after high temperature annealing. The oxidation temperature increased as SiC content increased. Thus, the protective effect against oxidation conferred by SiC coating on the CNT surface is dependent on the SiC content.

3.5. Wettability

The contact angle was determined by a sessile drop method, as shown in Fig. 6 [26]. An aluminum droplet was placed on the pristine MWCNT pellet (left) and SiC/CNT (right). The SiC/CNT was fabricated at a mixing ratio of 6:5. The droplet was maintained at 800 °C for 5 min in order to prevent interfacial reaction between carbon and aluminum, which modifies the contact angle [15]. The contact angle was further characterized by measuring the angle of the interface edge between the pellet and aluminum droplet, which is a triple point of the solid/liquid/vapor interface, as shown in the white box in Fig. 6a. Contact angles of the pristine CNTs (θ_{CNT}) and SiC/CNT (θ_{SiC}) pellet are shown in Fig. 6b and c, respectively. In order to improve reliability, several different views were used to characterize the contact angle, as summarized in Table 1. The average contact angle of θ_{CNT} was 145.8°, which is similar to previously reported values [15]. By incorporating a SiC layer, however, the θ_{SiC} was reduced to 134.6°, indicating improvement of Al

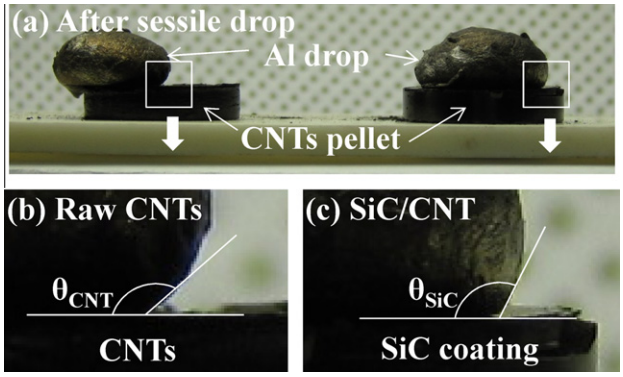

Fig. 6. Contact angle measurement after sessile drop of aluminum at 800 °C in vacuum at 10^{-2} torr. (a) Optical image after sessile drop of aluminum on a pristine CNT pellet (left) and SiC/CNT pellet (right). Contact angle measurement of (b) a pristine CNT pellet and (c) SiC/CNT pellet.

Table 1
Contact angle at different views after sessile drop at 800 °C.

View direction	Front	Left	Right	Average	Work of adhesion (W_a) (mJ/m^2)
θ_{CNT} (°)	145.2	143.3	148.9	145.8 (±1.6)	145
θ_{SiC} (°)	143.0	132	128.7	134.6 (±4.3)	253

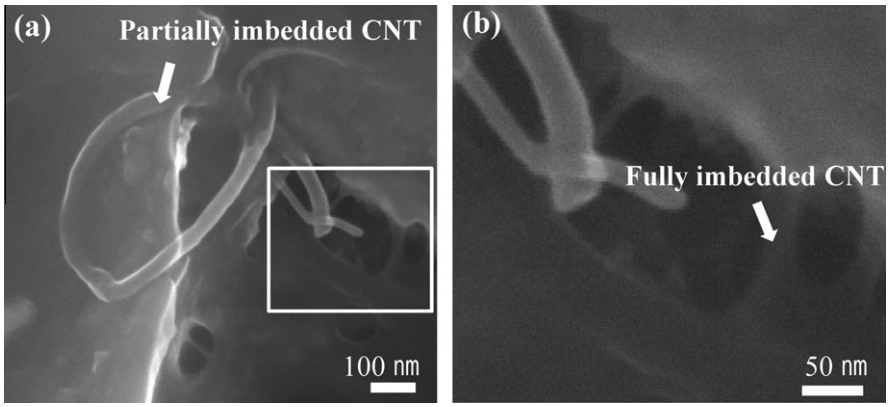

Fig. 7. SEM image of CNTs after wetting in aluminum at 700 °C showing different morphologies of embedded CNTs: (a) partially imbedded CNT and (b) fully imbedded CNT on the aluminum surface.

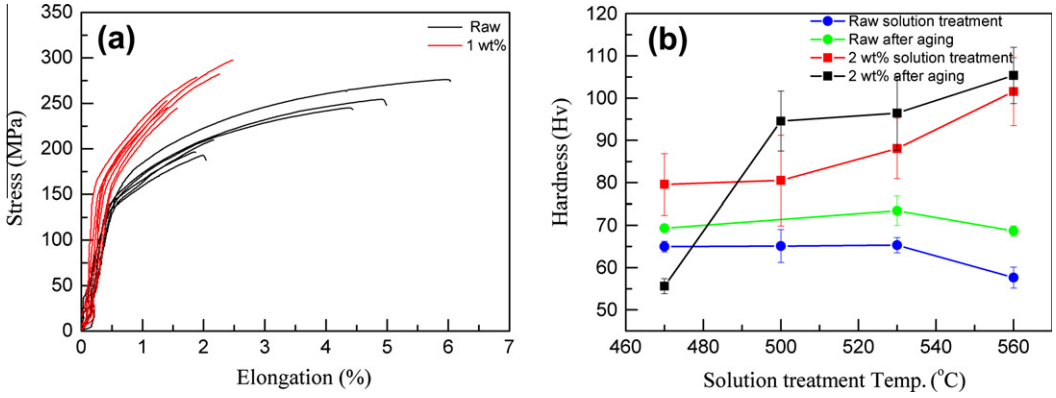

Fig. 8. Mechanical properties of the commercial A356.2 aluminum alloy incorporated with SiC/CNT. (a) strain–stress curve at 1 wt% of SiC/CNT. (b) Vickers hardness test depending on solution treatment temperature.

wetting on CNTs. The bonding force between the Al liquid and CNT solid phase, the work of adhesion, W_a, is defined by Young-Dupre equation [27].

$$W_a = \gamma_{lv}(1 + \cos\theta) \quad (1)$$

where $\gamma_{lv} \approx 850$ mJ/m^2 is the specific energy of liquid–vapor interface [28]. The calculated values of work of adhesion are 145 mJ/m^2 for raw CNTs and 253 mJ/m^2 for SiC/CNTs. By introducing SiC layer, 74% of adhesion force improvement was obtained. Hence strong interfacial bonding was expected by SiC layer formation resulting improved load transfer to CNTs.

In order to assess the wetting of aluminum, SiC/CNT powder was utilized instead of the pellet. It is known that a certain level of Si and Mg in pure Al yields improved wetting behavior [29]. Therefore, A356.2 aluminum alloy was used in this work, which contains Si 6.5% and Mg 0.3%, and it is expected to enhance the wettability of aluminum to SiC/CNT powder. Fig. 7 shows an SEM image acquired after an aluminum drop on the SiC/CNT powder at 700 °C for an hour in 10^{-6} torr vacuum. The SEM image was taken from the surface of the aluminum droplet. CNTs were detected on the surface of the aluminum. An important point related to this observation is that some parts of the CNTs were partially and fully

Table 2
Mechanical properties of 1 wt% CNT/A 356.2 composite after die-casting.

	Tensile strength (MPa)	Yield strength (MPa)	Young's modulus (GPa)	Elongation (%)
Raw A356.2	229 (±14)	150 (±3.6)	39 (±3.6)	2.8 (±0.56)
1 wt% CNT	265 (±8.4)	187 (±3.7)	70 (±7.1)	1.7 (±0.15)

embedded inside the aluminum, as shown in Fig. 7a and b, respectively, which provided improved wettability of aluminum to CNTs via SiC formation.

3.6. Mechanical properties of SiC/CNT-A356.2 composite

The mechanical properties were measured by incorporating SiC/CNT into the A356.2 commercial aluminum alloy by dissolving SiC/CNTs in aluminum via a melt blending technique. Before melt blending, SiC/CNT was premixed with pure aluminum powder by ball milling. This premixing treatment provides high dispersion of CNTs and high density for melt blending. At the same time, the surface gas adsorbate layer, which is a crucial obstacle in enhancing the wettability of nanomaterials, could be removed by mechanical ball milling [26]. The melt blending was done in our specially designed mechanical stirring system. A graphite impeller was introduced in the stirring system in order to mechanically disperse the premixture in liquid A356.2. Stirring was performed with a rotation speed of 500 rpm at 650 °C in vacuum. The concentrations of SiC and CNTs were 1.2 and 1 wt%, respectively. A standard tensile specimen (ASTM E 8 M-08) was fabricated using a die-casting technique.

Fig. 8a shows the stress–strain curve of the tensile specimen. By adding 1 wt% CNTs, improved mechanical properties such as Young's modulus, yield strength, and tensile strength were obtained. Table 2 summarizes the values obtained from Fig. 8a. The improvement was found to be 15% for tensile strength, 25% for yield strength and 79% for Young's modulus. However, elongation was decreased from 2.8% to 1.7%, as expected from the reinforced metal composite materials [6]. Previous work on mixing SiC powder with A356 by a stir casting technique followed by die casting is similar to our process, and this technique resulted in an ultimate tensile strength increase around 10% after the addition of 5 vol% (about 6 wt%) SiC [30]. The improvement reported in that study was lower than that observed our investigation. The reason for the high improvement in tensile strength in our case is ascribed to the addition of a SiC coating to the CNTs, which was expected to enhance the interfacial strength.

Hardness was also measured after T6 heat treatment (Fig. 8b). The concentrations of SiC and CNTs were 2.4 and 2 wt%, respectively. The hardness value decreased after aging in 470 °C of solution treatment with the addition of 2 wt% CNTs. These heat treatment conditions may not be appropriate for this SiC/CNT composite system; however, the hardness increased as the solution treatment temperature increased. This finding might be interpreted as prevention of solute dissolution by nano-sized reinforcement, suggesting that high temperature is required for uniform solution treatment. The highest hardness was obtained after aging with 560 °C solution treatment, yielding a 50% improvement in hardness compared to that of A356.2. The obtained value was also higher than the 73.6 Hv at 5 vol% of SiC [30]. Further details regarding the mechanism will be discussed in the future.

4. Conclusion

To reinforce aluminum, a SiC layer was formed on the CNT surface by a high temperature annealing process. The process involves mixing of mechanically crushed Si powder and CNT flakes with additional CNTs, followed by high temperature annealing. The morphology and microstructure of a SiC layer on the CNT surface were characterized by SEM and TEM. X-ray diffraction results indicated the successful formation of a SiC lattice. TGA results showed that the CNT oxidation temperature increased with SiC layer formation. Contact angle measurements after sessile drop indicated that the SiC layer reduced the contact angle of the Al droplet, improving the wettability of CNTs in aluminum. The wetting test eventually showed partial wetting of SiC/CNT into melted Al. Mechanical properties were investigated after SiC/CNT-A356.2 fabrication via a melt blending technique. The tensile strength and Young's modulus improved by 15% and 79%, respectively, after the addition of 1 wt% CNTs.

Acknowledgements

This research was supported by a grant from the Industrial Technology Development Programs of the Korea Institute of Energy Technology Evaluation and Planning (70004134) funded by the Korean government, Ministry of Knowledge Economy, and by the Star Faculty (No. 2010-0029653) and WCU Programs (2008-000-10029-0) of the NRF, funded by the MEST of Korea.

References

[1] Salvetat J-P, Bonard J-M, Thomson NH, Kulik AJ, Forío L, Benoit W, et al. Mechanical properties of carbon nanotubes. Appl Phys A 1999;69:255.
[2] Fujii M, Zhang X, Xie H, Ago H, Takahashi K, Ikuta T, et al. Measuring the thermal conductivity of a single carbon nanotube. Phys Rev Lett 2005;95:65502.
[3] Ebbesen TW, Lezec HJ, Hiura H, Bennet JW, Gaemi HF, Thio T. Electrical conductivity of individual carbon nanotubes. Nature 1996;382:54.
[4] Tjong SC. Structural and mechanical properties of polymer nanocomposites. Mater Sci Eng R 2006;53:73.
[5] Kim KT, Cha SI, Hong SH. Hardness and wear resistance of carbon nanotube reinforced Cu matrix nanocomposites. Mater Sci Eng A: Struct 2007;449:46.
[6] Kim KT, Cha SI, Hong SH. Microstructures and tensile behavior of carbon nanotube reinforced Cu matrix nanocomposites. Mater Sci Eng A: Struct 2006;430:27.
[7] Wang X, Padture NP, Tanaka H. Contact-damage-resistant ceramic/single-wall carbon nanotubes and ceramic/graphite composites. Nat Mater 2004;3:539.
[8] Wills W, Rovere ELL. Light vehicle energy efficiency programs and their impact on Brazilian CO_2 emissions. Energy Policy 2010;38:6453.
[9] Landry K, Kalogeropoulou S, Eustathopoulos N. Wettability of carbon by aluminum and aluminum alloys. Mater Sci Eng A: Struct 1998;254:99.
[10] Ci L, Ryu Z, Jin-Phillipp NY, Rühle M. Acta Mater 2006;54:5367.
[11] Lau T-K, Hui D. Effectiveness of using carbon nanotubes as nano-reinforcements for advanced composite structures. Carbon 2002;40:1605.
[12] Esawi AMK, Borady MAE. Carbon nanotube-reinforced aluminum strips. Compos Sci Technol 2008;68:486.
[13] Molina JM, Voytovych R, Louisa E, Eustathopoulos N. The surface tension of liquid aluminium in high vacuum: the role of surface condition. Int J Adhes Adhes 2007;27:394.
[14] Nuriel S, Liu L, Barber AH, Wagner HD. Direct measurement of multiwall nanotube surface tension. Chem Phys Lett 2005;404:263.
[15] Landry K, Kalotgeropoulou S, Eustathopoulos N. Wettability of carbon by aluminum and aluminum alloys. Mater Sci Eng A: Struct 1998;254:99.
[16] Ci L, Ryu Z, Jin-Phillipp NY, Ruhle M. Investigation of the interfacial reaction between multi-walled carbon nanotubes and aluminum. Acta Mater 2006;54:5367.
[17] Deng CF, Zhang XX, Wang DZ, Ma YX. Calorimetric study of carbon nanotubes and aluminum. Mater Lett 2007;61:3221.
[18] Laurent V, Rado C, Eustathopoulos N. Wetting kinetics and bonding of Al and Al alloys on α-SiC. Mater Sci Eng A: Struct 1996;205:1.
[19] Kim IH, Lee W, Lee CW, Ko SH, Jang JM. Effect of SiC coating on interfacial reaction between carbon short fiber and A melt. Surf Interface Anal 2010;42:743.
[20] Lee CW, Kim IH, Lee W, Ko SH, Jang JM, Lee TW, et al. Formation and analysis of SiC coating layer on carbon short fiber. Surf Interface Anal 2010;42:1231.
[21] Laha T, Kuchibhatla S, Seal S, Li W, Agarwal A. Interfacial phenomena in thermally sprayed multiwalled carbon nanotube reinforced aluminum nanocomposites. Acta Mater 2007;55:1059.
[22] Bakshi SR, Keshri AK, Singh V, Seal S, Agarwal A. Interface in carbon nanotube reinforced aluminum silicon composites: Thermodynamic analysis and experimental verification. J Alloy Compd 2009;481:207.
[23] Xi G, Peng Y, Wan S, Li T, Yu W, Qian Y. Lithium-assisted synthesis and characterization of crystalline 3C–SiC nanobelts. J Phys Chem B 2004;108:20102.
[24] Wang Y, Zerda TW. The mechanism of the solid-state reaction between carbon nanotubes and nanocrystalline silicon under high pressure and at high temperature. J Phys: Condens Matter 2006;18:2995.
[25] So KP, Kim ES, Biswas C, Joeng HY, Keum DH, An KH, et al. Low-temperature solid state dissolution of carbon atoms into aluminum nanoparticles. Scripta Mater 2012;66:21.
[26] Hashim J, Looney L, Hashmi MSJ. The wettability of SiC particles by molten aluminium alloy. J Mater Process Technol 2001;119:324.
[27] Young T. An essay on the cohesion of fluids. Trans R Soc 1805;95:65.

[28] Keene BJ. Review of data for the surface tension of pure metals. Int Mater Rev 1993;38:157.
[29] Janghorban K. Investigation of the effects of silicon and carbon on the phase composition of SiC–Al composites. Compos Sci Technol 1994;50:299.
[30] Tzamtzis S, Barekar NS, Babu NH, Patel J, Dhindaw BK, Fan Z. Processing of advanced Al/SiC particulate metal matrix composites under intensive shearing – a novel Rheo-process. Compos Part A–Appl Sci Manuf 2009;40:144.